Non-Orthogonal Moving Frame for the Kinematics of Parallel Pointing Mechanisms

Bai, Shaoping

Published in:
IEEE Robotics and Automation Letters

DOI (link to publication from Publisher):
10.1109/LRA.2023.3235192

Publication date:
2023

Document Version
Accepted author manuscript, peer reviewed version

Non-orthogonal moving frame for the kinematics of parallel pointing mechanisms

Shaoping Bai

***Abstract*—A non-orthogonal frame is proposed in this work as an alternative representation of moving frames, which can describe naturally and conveniently orientations of the mobile platform of parallel pointing mechanisms. Fundamentals of non-orthogonal bases are presented, upon which a non-orthogonal frame is established utilizing two body-attached vectors and their bivector. Properties of the non-orthogonal frame are analyzed geometrically and algebraically. With the alternative representation, we revisit the kinematics of parallel pointing mechanisms. Efficient and robust kinematic formulations are obtained and demonstrated with examples.**

***Index Terms*—Kinematics, parallel pointing mechanisms, non-orthogonal frame, Jacobian of pointing, spherical parallel manipulators**

I. Introduction

ROTATION matrix is a classic mathematical tool to transform coordinates within two coordinate frames and to describe rigid-body rotation. According to Euler's Theorem, a rigid-body rotation, or simply a rotation, is represented by a 3×3 proper orthogonal matrix. Many types of parameters can be used to express rotation matrix, such as Euler angles, Euler parameters, natural invariants, etc.[1], [2], [3], [4]. For all representations, at least three parameters are needed.

While rotation matrix is widely used in kinematics and robotics, a limitation to represent spatial rotation is noted for mechanisms with lower mobility, namely, with rotation of 1-DOF (degree-of-freedom) or 2-DOF rotations. Ideally, the rotation matrix for these type of mechanisms should correspondingly have 1 or 2 parameters to match the number of DOF. Unfortunately, any aforementioned representation of rotation matrix contains parameters, for example, three Euler angles, that are more than needed. Parameter redundancy exist, i.e., the number of variables in constraint equations is more than the number of DOFs. The redundancy implies issues such as low efficiency and robustness, which calls for new formulations for mechanisms with fewer mobility, in particular, spherical pointing mechanisms (PPM) in this study.

The PPMs are mechanisms to generate 2-DOF rotation with respect to desired longitude and latitude [5], [6]. Pointing mechanisms have a wide range of applications, such as five-axis machining tools [7], solar panel tracker [8], micro assembly cell [9], robotic wrist [10], antennas tracking [6], etc. Some recent designs can be found in [11], [12], [13]. The PMMs are essentially spherical parallel manipulators. Unlike most spherical parallel manipulators (SPM) of 3-DOFs [14], [15], [16], [17], the PPMs carry their mobile platforms for 2-DOF rotation while involving rotations in all three axes [9]. When the rotation of the mobile platform is described by Euler angles or the similar, parameter redundance exists.

In this work, we propose a representation of moving frame by means of non-orthogonal basis, which provides a natural alternative to describe uniquely and effectively the orientation of a moving rigid body. A non-orthogonal frame (NOF) is established with two body-attached vectors and their bivector. The NOF formulation leads to a system of constraint equations with minimum parameters. This enables efficient equation solving and kinematic analysis, as revealed in this paper. The work is based on the author's previous work [18] with substantial extensions including (1) systematic treatment of the non-orthogonal moving frame, (2) pointing workspace and velocity analysis, (3) Jacobian matrices. Moreover, the method is extended to a 2-DOF PPM derived from a 3-DOF SPM, along with examples and comprehensive performance comparisons.

The balance of the paper is organized as follows. Section II introduces the NOF, established with non-orthogonal bases. Properties of the NOF are analyzed. In Sections III and IV, we revisit the kinematics of two PPMs, namely, a five-bar PPM and a PPM derived from 3-DOF SPM. In Sec. V, numerical examples are included to show the efficacy of the NOF. The work is discussed in Sec.VI and concluded in Sec.VII.

II. Alternative coordinate frame with a non-orthogonal basis

In this work, we attempt to establish a body attached frame with a non-orthogonal basis in $\mathbb{R}^3$. Some fundamentals of non-orthogonal bases can be found in Appendix A for readers' information [19].

A. Representation with non-orthogonal frames

A moving frame can be represented by either orthogonal or non-orthogonal bases. With non-orthogonal bases considered, there are many choices for the moving body frame. As our objective is to use minimum parameters for the moving frame, we thus select two non-parallel unit vectors from a moving body and their bivector. Refer to Fig. 1, we assume that two

Manuscript received: September 4, 2022; Revised: November 21, 2022; Accepted: December 28, 2022.

This paper was recommended for publication by Editor Lucia Pallottino upon evaluation of the Associate Editor and Reviewers' comments.

The work is partly supported by Independent Research Fund Denmark(DFF) through VIEXO project.

S. Bai is with Department of Materials and Production, Aalborg University, Aalborg 9220, Denmark (email: shb@mp.aau.dk).

Digital Object Identifier (DOI): see top of this page

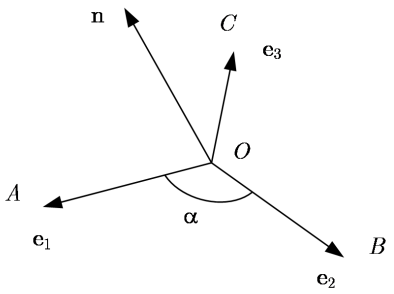

Fig. 1. A non-orthogonal moving frame with two vectors and their bivector

unit vectors $\mathbf{e}_1$ and $\mathbf{e}_2$ are known. A non-orthogonal frame (NOF) can hence be established with $\mathbf{e}_1$, $\mathbf{e}_2$ and $\mathbf{e}_3 = \mathbf{e}_1 \times \mathbf{e}_2$. They are linearly independent and form a basis of $\mathbb{R}^3$.

With the NOF, any vector $\mathbf{n} \in \mathbb{R}^3$ can be expressed as

$$\mathbf{n} = \mu\mathbf{e}_1 + \nu\mathbf{e}_2 + \lambda\mathbf{e}_3 \tag{1}$$

or

$$\mathbf{n} = \mathbf{M}\mathbf{n}^\star \tag{2}$$

with

$$\mathbf{M} = [\mathbf{e}_1, \mathbf{e}_2, \mathbf{e}_3], \quad \mathbf{n}^\star = [\mu, \nu, \lambda]^T \tag{3}$$

where μ, ν and λ are dimensionless parameters. In this formulation, $\mathbf{M}$ is the matrix corresponding to the NOF, or NOF matrix in short. $\mathbf{n}^\star$ is a vector containing coordinates associated with vector $\mathbf{n}$, which is referred as the set of *alternative coordinates*.

The inverse of the NOF matrix is readily obtained from the reciprocal vectors of $\mathbf{e}_i$. Let $\mathbf{e}^i, i = 1, 2, 3$ be the reciprocal vectors, as defined by eq. (69), and $\check{\mathbf{M}}$ be the reciprocal matrix,

$$\check{\mathbf{M}} = [\mathbf{e}^1, \mathbf{e}^2, \mathbf{e}^3] \tag{4}$$

We can readily show that

$$\check{\mathbf{M}}^T\mathbf{M} = \mathbf{I} \tag{5}$$

where $\mathbf{I}$ stands for the 3×3 identity matrix. We thus have

$$\mathbf{M}^{-1} = \check{\mathbf{M}}^T \tag{6}$$

The alternative coordinates can hence be found by

$$\mathbf{n}^\star = \mathbf{M}^{-1}\mathbf{n} = \check{\mathbf{M}}^T\mathbf{n} \tag{7}$$

The alternative coordinates can also be found geometrically. By premultiplying both sides of eq. (1) with $\mathbf{e}_1^T$, $\mathbf{e}_2^T$, and $\mathbf{e}_3^T$ separately and solving the equations, we obtain

$$\mu = k(\cos\beta_1 - \cos\beta_2 \cos\alpha) \tag{8a}$$

$$\nu = k(\cos\beta_2 - \cos\beta_1 \cos\alpha) \tag{8b}$$

$$\lambda = kp \tag{8c}$$

where $k = 1/\sin^2\alpha, p = (\mathbf{e}_1 \times \mathbf{e}_2)^T\mathbf{n}$. $\alpha \in [0, \pi]$ is the angle made by $\mathbf{n}_1$ and $\mathbf{n}_2$, while β_1 and β_2 are angles made by $\mathbf{n}$ and $\mathbf{e}_1$, $\mathbf{n}$ and $\mathbf{e}_2$, respectively. These geometric identities show that the alternative coordinates are determined purely from geometric relations of three vectors. They are invariants and hence frame independent.

B. Geometric and algebraic properties of NOF

The NOF is an alternative to the conventional orthonormal bases representation, or rotation matrix. Relationships between the NOF and the rotation matrix are thus revealed.

Algebraically, a rotation matrix $\mathbf{Q}$ in n-dimensions is a $n \times n$ special orthogonal matrix, namely,

$$\mathbf{Q}^T\mathbf{Q} = \mathbf{I}; \quad \det(\mathbf{Q}) = 1 \tag{9}$$

Matrix $\mathbf{Q}$ can also represent the orientation of a mobile platform (MP), which stands for the transformation from the base frame, denoted by $\mathcal{B}$, to the MP attached body frame, denoted by $\mathcal{A}$. In such a case, frame $\mathcal{A}$ is selected to be coincident with the base frame $\mathcal{B}$ at the initial posture.

For the NOF matrix, it has to be noted that both conditions of (9) are not satisfied. Instead, we have $\det(\mathbf{M}) = \sin^2\alpha$.

Matrix $\mathbf{M}$ can be converted to $\mathbf{Q}$, and vice versa, as described presently.

Let $\mathbf{Q} = [\mathbf{e}_x, \mathbf{e}_y, \mathbf{e}_z]$. Vectors for the NOF frame are then expressed as

$$\mathbf{e}_i = c_{i1}\mathbf{e}_x + c_{i2}\mathbf{e}_y + c_{i3}\mathbf{e}_z = \mathbf{Q}\mathbf{c}_i, \quad i = 1, 2, 3 \tag{10}$$

where $c_{ij}, j = 1, 2, 3$ are real coefficients. We thus have

$$\mathbf{M} = \mathbf{Q}[\mathbf{c}_1, \mathbf{c}_2, \mathbf{c}_3] = \mathbf{Q}\mathbf{C} \tag{11}$$

where $\mathbf{C}$ is a matrix mapping the conventional rotation matrix to the NOF. The mapping matrix can be found algebraically as

$$\mathbf{C} = \mathbf{Q}^{-1}\mathbf{M} = \mathbf{Q}^T\mathbf{M} \tag{12}$$

It is known that for any vector $\mathbf{s}$ in the base frame $\mathcal{B}$, when expressed in frame $\mathcal{A}$, the following relation holds,

$$\mathbf{s} = \mathbf{Q}\mathbf{s}' \tag{13}$$

where $\mathbf{s}'$ is the local vector of $\mathbf{s}$.

On the other hand, the same vector can be expressed in the NOF with alternative coordinates, noted by $\mathbf{s}^\star$, as

$$\mathbf{s} = \mathbf{M}\mathbf{s}^\star = \mathbf{Q}\mathbf{C}\mathbf{s}^\star \tag{14}$$

from which we find a useful identity

$$\mathbf{s}' = \mathbf{C}\mathbf{s}^\star \tag{15}$$

As can be seen form the above equation, the ordinary local coordinates and the alternative coordinates are related by the mapping matrix $\mathbf{C}$ too.

The differential kinematics with the NOF has a similar form as the rotation matrix. Taking time derivatives on both sides of eq. (11) yields

$$\dot{\mathbf{M}} = \dot{\mathbf{Q}}\mathbf{C} \tag{16}$$

As $\dot{\mathbf{Q}} = \widetilde{\boldsymbol{\omega}}\mathbf{Q}$, the equation becomes

$$\dot{\mathbf{M}} = \widetilde{\boldsymbol{\omega}}\mathbf{Q}\mathbf{C} \tag{17}$$

where the sign '$\sim$' on top of a vector denotes the *skew symmetric matrix* derived from the vector. Finally, we have

$$\dot{\mathbf{M}} = \widetilde{\boldsymbol{\omega}}\mathbf{M} \tag{18}$$

which remains the same form as the Poisson equation of the rigid-body rotation.

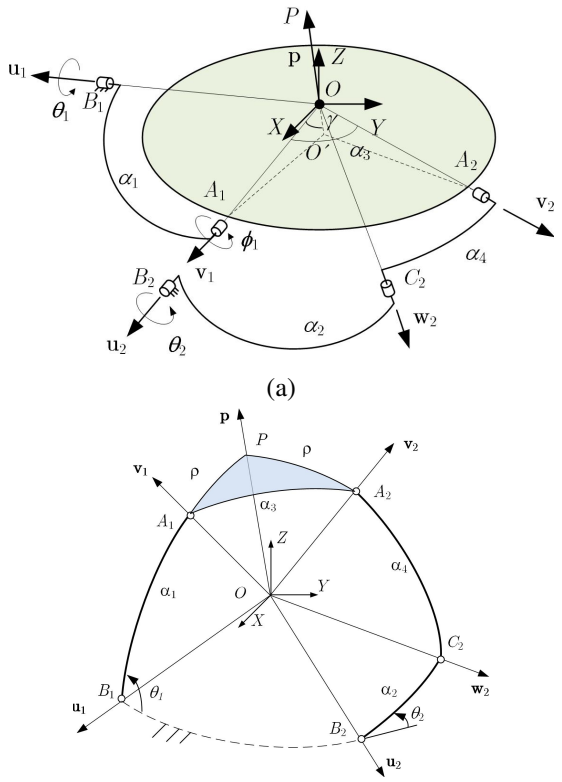

Fig. 2. A spherical pointing mechanism centered at point O, (a) kinematic parameters, (b) an equivalent 5-bar mechanism (not drawn to scale), where $\rho = \pi - \gamma$.

III. NOF FOR A FIVE-BAR 2-DOF SPHERICAL PPM

With the NOF introduced, we revisit the kinematics of a 2-DOF PPM shown in Fig. 2a. Without loss of generality, we assume its mobile platform is a cone with its half angle specified by γ, which is generated by sweeping OA_1 about OO', with O being its apex and OO' parallel to the point vector. Moreover, OA_2 lies on the conical surface for a symmetric shape of the mobile platform.

The PPM is essentially a five-bar spherical linkage, as shown Fig. 2b. This five-bar PPM has two limbs. The first limb of single curved link B_1A_1 has a dimension of α_1, the second limb of two curved links B_2C_2 and C_2A_2 having dimensions of α_2 and α_4, respectively. The two revolute joints B_1 and B_2 on the fixed base are described by unit vectors $\mathbf{u}_1$ and $\mathbf{u}_2$, while the two revolute joints A_1 and A_2 on the moving platform are described by unit vectors $\mathbf{v}_1$ and $\mathbf{v}_2$, respectively. The unit vector parallel to the axis of the revolute joint C_2 is denoted by $\mathbf{w}_2$. The pointing direction is denoted by a unit vector $\mathbf{p} = [x, y, z]^T$, its magnitude unity implying

$$g(x, y, z) = x^2 + y^2 + z^2 - 1 = 0 \tag{19}$$

For pointing mechanisms, the pointing direction is conventionally expressed with *spherical coordinates*, namely, *longitude* and *latitude*, which describe uniquely the pan and tilt motion of the mechanism. Let ϕ_p and φ_p be the longitude and the latitude, or more exactly, the *angles of pointing*, then

$$\mathbf{p} = \begin{bmatrix} \cos\varphi_p \cos\phi_p \\ \cos\varphi_p \sin\phi_p \\ \sin\varphi_p \end{bmatrix}, \quad \phi_p \in [-\pi, \pi],\ \varphi_p \in [-\frac{\pi}{2}, \frac{\pi}{2}] \tag{20}$$

Spherical coordinates have coordinate singularity with $\varphi_p = \pm\pi/2$. Care has to be taken as ϕ_p will then not uniquely determined from pointing vectors in Cartesian coordinates.

A. Kinematic constraint equations

A NOF is established at the mobile platform with $\mathbf{p}$, $\mathbf{v}_1$, and their bivector $\mathbf{p} \times \mathbf{v}_1$, as shown in Fig. 2b. The NOF matrix is

$$\mathbf{M} = [\mathbf{p}, \mathbf{v}_1, \mathbf{p} \times \mathbf{v}_1] \tag{21}$$

We start our formulation from the first limb B_1A_1. The link rotates about a fixed axis for an angle θ_1,

$$\mathbf{v}_1 = \mathbf{R}_1 \mathbf{v}_{10} \tag{22}$$

where $\mathbf{v}_{10}$ is the unit vector parallel to the initial position of OA_1. Moreover, matrix $\mathbf{R}_1$ describes the rotation of link B_1A_1 about OB_1. Using *natural invariants* of the rigid-body rotation, matrix $\mathbf{R}_1$ takes the form [20]

$$\mathbf{R}_i = \mathbf{u}_i \mathbf{u}_i^T + \sin\theta_i \tilde{\mathbf{u}}_i + \cos\theta_i (\mathbf{I} - \mathbf{u}_i \mathbf{u}_i^T), i = 1, 2 \tag{23}$$

For the second limb, curved link B_2C_2 rotates about the axis OB_2, the unit vector $\mathbf{w}_2$ is expressed as

$$\mathbf{w}_2 = \mathbf{R}_2 \mathbf{w}_{20} \tag{24}$$

where $\mathbf{w}_{20}$ is the unit vector parallel to OC_2 at the reference position and $\mathbf{R}_2$ is a rotation matrix defined by eq. (23).

We now need to express the unit vector $\mathbf{v}_2$. Conventionally, we have to use the rotation matrix of the mobile platform expressed with either Euler angles or the joint angles θ_1 and ϕ_1. In any case, intermediate variables have to be included. With the NOF matrix, we can directly express $\mathbf{v}_2$ as

$$\mathbf{v}_2 = \mathbf{M}\mathbf{v}_2^\star, \quad \mathbf{v}_2^\star = [\mu_2, \nu_2, \lambda_2]^T \tag{25}$$

which is free of intermediate variables.

The first constraint equation is hence formulated upon vector $\mathbf{v}_1$,

$$\mathbf{v}_1^T \mathbf{p} = \cos\rho \tag{26}$$

The second constraint equation is formulated for the second limb,

$$\mathbf{w}_2^T \mathbf{v}_2 = \cos\alpha_4 \tag{27}$$

Equations (26) and (27) stand for the system of constraint equations of the 2-DOF pointing mechanism. The system contains two input angles and the unit pointing vector $\mathbf{p}$. In other words, the system uses minimum number of parameters, namely, only two, for the 2-DOF mechanism. The system allows us to solve directly the forward position problem for any specified angles of θ_1 and θ_2, or the inverse position problem with a specified pointing vector.

The inverse and forward position problems admit different numbers of solutions, as revealed presently.

Equation (27) is first expanded as,

$$\mathbf{w}_2^T[\mu_2\mathbf{p} + \nu_2\mathbf{v}_1 + \lambda_2(\mathbf{p}\times\mathbf{v}_1)] = \cos\alpha_4 \tag{28}$$

that is

$$\mathbf{w}_2^T[(\mu_2\mathbf{I} - \lambda_2\tilde{\mathbf{v}}_1)\mathbf{p} + \nu_2\mathbf{v}_1] = \cos\alpha_4 \tag{29}$$

which is rewritten as

$$\mathbf{q}^T\mathbf{p} = \cos\alpha_4 - \nu_2\mathbf{w}_2^T\mathbf{v}_1 \tag{30}$$

where

$$\mathbf{q} = \mu_2\mathbf{w}_2 + \lambda_2(\mathbf{v}_1\times\mathbf{w}_2) \tag{31}$$

It can be seen that both eqs. (26) and (30) are linear equations of $\mathbf{p}$. As $\mathbf{p}$ is a unit vector subject to eq. (19), the Bezout number of the whole system of constraint equations is equal to 2. The forward position problem thus admits maximum two real solutions.

In the inverse problem, the pointing vector $\mathbf{p}$ is given. Eq. (26) can be written in the form of

$$A_1\cos\theta_1 + B_1\sin\theta_1 + C_1 = 0 \tag{32}$$

which admits two solutions of θ_1. Equation (27) can then be written in terms of θ_2 similar to eq. (32). Two solutions of θ_2 will be found for each value of θ_1. The inverse position problem thus admits four solutions.

In summary, *the five-bar PPM of general kinematic structure admits maximum two forward and four inverse real solutions.*

B. Jacobian matrices

The Jacobian matrix of the pointing mechanism is readily obtained from the two constraint equations (26) and (27).

Differentiating both sides of eq. (26) yields

$$\mathbf{v}_1^T\dot{\mathbf{p}} + \mathbf{p}^T\dot{\mathbf{v}}_1 = 0 \tag{33}$$

Note that

$$\dot{\mathbf{p}} = \boldsymbol{\omega}\times\mathbf{p};\ \dot{\mathbf{v}}_1 = \dot{\boldsymbol{\theta}}_1\times\mathbf{v}_1 \tag{34}$$

we have

$$\mathbf{v}_1^T(\boldsymbol{\omega}\times\mathbf{p}) + \mathbf{p}^T(\dot{\boldsymbol{\theta}}_1\times\mathbf{v}_1) = 0 \tag{35}$$

where $\dot{\boldsymbol{\theta}}_1 = \dot{\theta}_1\mathbf{u}_1$. The above equation is finally rewritten as

$$\mathbf{v}_1^T(\mathbf{p}\times\boldsymbol{\omega}) - \mathbf{p}^T(\mathbf{u}_1\times\mathbf{v}_1)\dot{\theta}_1 = 0 \tag{36}$$

Similarly, differentiating eq. (27) yields

$$\dot{\mathbf{w}}_2^T\mathbf{v}_2 + \mathbf{w}_2^T\dot{\mathbf{v}}_2 = 0 \tag{37}$$

With

$$\dot{\mathbf{w}}_2 = \dot{\boldsymbol{\theta}}_2\times\mathbf{w}_2,\ \dot{\mathbf{v}}_2 = \dot{\boldsymbol{\omega}}\times\mathbf{v}_2 \tag{38}$$

where $\dot{\boldsymbol{\theta}}_2 = \dot{\theta}_2\mathbf{u}_2$, eq. (37) is rewritten as

$$(\dot{\boldsymbol{\theta}}_2\times\mathbf{w}_2)^T\mathbf{v}_2 + \mathbf{w}_2^T(\boldsymbol{\omega}\times\mathbf{v}_2) = 0 \tag{39}$$

or

$$\mathbf{w}_2^T(\mathbf{v}_2\times\boldsymbol{\omega}) - \mathbf{v}_2^T(\mathbf{u}_2\times\mathbf{w}_2)\dot{\theta}_2 = 0 \tag{40}$$

Equations (36) and (40) are written in a matrix form

$$\mathbf{J}_A\boldsymbol{\omega} = \mathbf{J}_B\dot{\boldsymbol{\theta}},\quad \boldsymbol{\theta} = [\theta_1,\theta_2]^T \tag{41}$$

where

$$\mathbf{J}_A = \begin{bmatrix} \mathbf{v}_1^T\tilde{\mathbf{p}} \\ \mathbf{w}_2^T\tilde{\mathbf{v}}_2 \end{bmatrix} \in \mathbb{R}^{2\times3} \tag{42}$$

$$\mathbf{J}_B = \begin{bmatrix} \mathbf{p}^T(\mathbf{u}_1\times\mathbf{v}_1) & 0 \\ 0 & \mathbf{v}_2^T(\mathbf{u}_2\times\mathbf{w}_2) \end{bmatrix} \in \mathbb{R}^{2\times2} \tag{43}$$

which is the velocity equation of the 2-DOF PPM.

Assuming $\mathbf{J}_B$ invertible, the input velocity for any given angular velocity $\boldsymbol{\omega}$ of the mobile platform can be calculated by

$$\dot{\boldsymbol{\theta}} = \mathbf{J}_B^{-1}\mathbf{J}_A\boldsymbol{\omega} \tag{44}$$

However, eq. (41) does not allow us to find uniquely the angular velocity of the mobile platform for given joint velocities. An additional equation is thus needed.

Referring to the first limb of the manipulator, we have

$$\boldsymbol{\omega} = \dot{\theta}_1\mathbf{u}_1 + \dot{\phi}_1\mathbf{v}_1 \tag{45}$$

where ϕ_1 is the angle of rotation at the passive joint A_1.

Premultiplying both sides with $\mathbf{u}_1\times\mathbf{v}_1$ yields

$$(\mathbf{u}_1\times\mathbf{v}_1)^T\boldsymbol{\omega} = 0 \tag{46}$$

Equation (41) is now expanded with eq. (46) as

$$\underline{\mathbf{J}}_A\boldsymbol{\omega} = \underline{\mathbf{J}}_B\dot{\boldsymbol{\theta}} \tag{47}$$

with

$$\underline{\mathbf{J}}_A = \begin{bmatrix} \mathbf{J}_A \\ (\mathbf{u}_1\times\mathbf{v}_1)^T \end{bmatrix} \in \mathbb{R}^{3\times3},\quad \underline{\mathbf{J}}_B = \begin{bmatrix} \mathbf{J}_B \\ 0 \end{bmatrix} \in \mathbb{R}^{3\times2} \tag{48}$$

which yields

$$\boldsymbol{\omega} = \mathbf{J}_r\dot{\boldsymbol{\theta}},\quad \mathbf{J}_r = \underline{\mathbf{J}}_A^{-1}\underline{\mathbf{J}}_B \in \mathbb{R}^{3\times2} \tag{49}$$

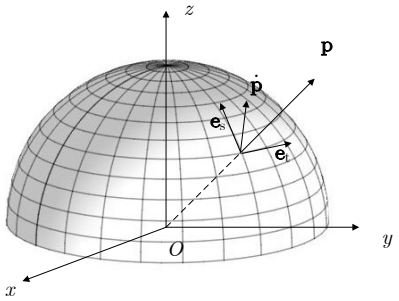

Fig. 3. Projection of velocity into the spherical tangential space.

We are able to find velocity of the mobile platform for any given velocities at active joints, or vise versa. An outstanding issue is then to find the pointing velocity, i.e., the changing rates of the pointing angles.

Differentiating both sides of eq. (20) with respect to time yields

$$\dot{\mathbf{p}} = \mathbf{A}\dot{\boldsymbol{\phi}}_p \tag{50}$$

where

$$\boldsymbol{\phi}_p = [\phi_p,\varphi_p]^T,\quad \mathbf{A} = \frac{\partial\mathbf{p}}{\partial\boldsymbol{\phi}_p} \in \mathbb{R}^{3\times2} \tag{51}$$

On the other hand

$$\dot{\mathbf{p}} = \boldsymbol{\omega} \times \mathbf{p} = -\tilde{\mathbf{p}}\boldsymbol{\omega} = \tilde{\mathbf{p}}^T \underline{\mathbf{J}}_A^{-1} \underline{\mathbf{J}}_B \dot{\boldsymbol{\theta}} \tag{52}$$

thus

$$\mathbf{A}\dot{\boldsymbol{\phi}}_p = \tilde{\mathbf{p}}^T \underline{\mathbf{J}}_A^{-1} \underline{\mathbf{J}}_B \dot{\boldsymbol{\theta}} \tag{53}$$

Equation (53) is an overdetermined system, as both $\dot{\boldsymbol{\phi}}_p$ and $\dot{\boldsymbol{\theta}}$ are two-dimensional, while their coefficient matrices are 3×2. It is desirable to convert it into a determined system. We notice that $\dot{\mathbf{p}}$ lies in the space spanned by orthogonal vectors $\mathbf{e}_t$ and $\mathbf{e}_s$ tangential to the unit sphere, as shown in Fig. 3. We thus can project the vector from the 3D Cartesian space to the 2D tangent space. To this end, we premultiply both sides of eq. (53) with $\mathbf{e}_t^T$ and $\mathbf{e}_s^T$ separately, which leads to

$$\mathbf{N}\mathbf{A}\dot{\boldsymbol{\phi}}_p = \mathbf{N}\tilde{\mathbf{p}}^T \underline{\mathbf{J}}_A^{-1} \underline{\mathbf{J}}_B \dot{\boldsymbol{\theta}} \tag{54}$$

or

$$\mathbf{J}_\phi \dot{\boldsymbol{\phi}}_p = \mathbf{J}_\theta \dot{\boldsymbol{\theta}} \tag{55}$$

where

$$\mathbf{J}_\phi = \mathbf{N}\mathbf{A} \in \mathbb{R}^{2\times 2}; \quad \mathbf{J}_\theta = \mathbf{N}\tilde{\mathbf{p}}^T \underline{\mathbf{J}}_A^{-1} \underline{\mathbf{J}}_B \in \mathbb{R}^{2\times 2} \tag{56}$$

with

$$\mathbf{N} = \begin{bmatrix} \mathbf{e}_t^T \\ \mathbf{e}_s^T \end{bmatrix}; \quad \mathbf{e}_t = \frac{\mathbf{p} \times \mathbf{z}}{||\mathbf{p} \times \mathbf{z}||}; \quad \mathbf{e}_s = \mathbf{p} \times \mathbf{e}_t \tag{57}$$

where $\mathbf{z}$ is the unit vector for the z axis. The velocity of pointing is finally obtained as

$$\dot{\boldsymbol{\phi}}_p = \mathbf{J}_p \dot{\boldsymbol{\theta}}; \quad \mathbf{J}_p = \mathbf{J}_\phi^{-1} \mathbf{J}_\theta \in \mathbb{R}^{2\times 2} \tag{58}$$

So far, we have formulated completely velocity equations for the PPM, i.e., eq. (58) to calculate the changing rate of pointing angles and (49) for the angular velocity of the mobile platform. To distinguish two Jacobian matrices, we refer $\mathbf{J}_r$ as the *Jacobian of rotation* and $\mathbf{J}_p$ as the *Jacobian of pointing*.

IV. NOF WITH A PPM DERIVED FROM 3-RRR SPM

The new method is extended to a 2-DOF PPM derived from 3-RRR SPM, as shown in Fig. 4, by fixing one input link, for example, link B_3C_3. The unit vectors $\mathbf{u}_i$, $\mathbf{v}_i$, and $\mathbf{w}_i$, for $i = 1, 2, 3$, are parallel to the axes of all joints. Moreover, the dimensions of the proximal links and the distal links, connected to the mobile platform, are angles α_1 and α_2, respectively. Angles θ_i are measured from the z-$\mathbf{u}_i$ plane.

With the NOF and alternative coordinates, we are able to establish kinematic constraint equations more efficiently. To this end, we take the NOF matrix as $\mathbf{M} = [\mathbf{p}, \mathbf{v}_3, \mathbf{p} \times \mathbf{v}_3]$, with which we have

$$\mathbf{v}_i = \mathbf{M}\mathbf{v}_i^\star, \quad i = 1, 2 \tag{59}$$

Vector $\mathbf{v}_3$ is rotated about $\mathbf{w}_3$ for ψ, which satisfies

$$\mathbf{p} \cdot \mathbf{v}_3 = \cos\beta \tag{60}$$

where β defines the shape of the mobile platform, as shown in Fig. 4. We thus have a system of three equations, namely, eq. (59) and (60), with only one intermediate variable ψ. Compared with the conventional formulations [21], [22], as outlined in Appendix B-B, which includes five equations, the NOF formulation has a smaller and simpler system of kinematic constraints, implying a big advantage of computation efficiency.

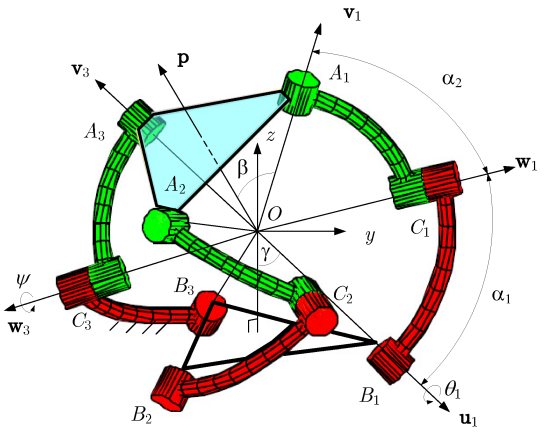

Fig. 4. A 2-DOF PPM derived from 3-RRR SPM with regular pyramid shape base and mobile platforms.

V. EXAMPLES

We include numerical examples to demonstrate the advantages of the kinematics with the NOF.

A. Position Analysis

The first example is position analysis of the five-bar PPM. In this example, the geometry is specified by $\mathbf{u}_1 = [1, 0, 0]^T$, $\mathbf{u}_2 = [0, 1, 0]^T$, and $\{\alpha_1, \alpha_2, \alpha_3, \alpha_4, \gamma\} = \{\pi/2, \pi/3, 13\pi/36, \pi/3, 7\pi/18\}$ radians. We let $\mathbf{p} = [0.3551, 0.0719, 0.9320]^T$. From eqs. (26) and (27), four inverse kinematic (IK) solutions are immediately found, as listed in Table I. Figure 5 displays all four configurations of the pointing mechanism for the four IK solutions.

TABLE I
INVERSE KINEMATIC SOLUTIONS (UNIT: RAD.)

No.	1	2	3	4
θ_1	-2.8441	-0.4516	-0.4516	-2.8441
θ_2	3.1173	1.1362	-1.2694	-1.7049

We further assign joint angles $(\theta_1, \theta_2) = (2.67, 3.35)$ rad for forward kinematic (FK) problem. Using eqs. (26) and (27) combining (19), two FK solutions $\mathbf{p} = [-0.5796, 0.6402, 0.5039]^T$, and $\mathbf{p} = [0.0376, 0.7307, 0.6816]^T$ were obtained. The number of solutions is consistent with our formulation.

To facilitate the workspace analysis of the five-bar PPM, we rewrite the two constraint equations (26) and (27) in the following form

$$A_i \cos\theta_1 + B_i \sin\theta_1 + C_i = 0 \tag{61}$$

where coefficients $A_i, B_i, C_i, i = 1, 2$, are functions of ϕ_p and φ_p. Moreover, A_2, B_2, C_2 are also functions of θ_2. The two equations and $\sin^2\theta_1 + \cos^2\theta_1 = 1$ lead to

$$\begin{aligned} &{A_1}^2{C_2}^2 - {A_1}^2{B_2}^2 - {A_2}^2{B_1}^2 + {A_2}^2{C_1}^2 + {B_1}^2{C_2}^2 \\ &+2(A_1A_2B_1B_2 - A_1A_2C_1C_2 - B_1B_2C_1C_2) + {B_2}^2{C_1}^2 = 0 \end{aligned} \tag{62}$$

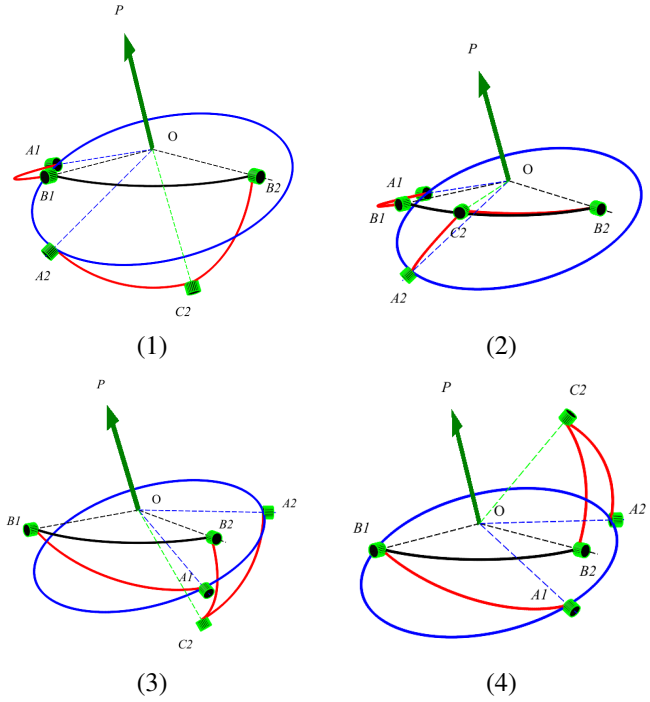

Fig. 5. Graphic display of the IK solutions, where figure numbers are corresponding to the solutions in Table I. In the figure, red curves are moving links, while the blue circle stands for the mobile platform, with a pointing vector in green normal to it.

This is an implicit equation of ϕ_p, φ_p and θ_2 and can be used to analyze either analytically or graphically the workspace of the PPM. For example, by substituting half-angle identities:

$$\cos\theta_2 = \frac{1-u^2}{1+u^2}; \quad \sin\theta_2 = \frac{2u}{1+u^2} \tag{63}$$

a quartic of u will be obtained. Root analysis of the polynomial can yield the workspace. Alternatively, the workspace can be displayed graphically. Figure 6 shows the pointing workspace of the mechanism. It was obtained with two steps. At first, we generate the surface of eq. (62) in 3D space; we then project the surface into the $\phi_p - \varphi_p$ plane, which gives the feasible workspace. As we can notice, this PPM is not able to point all directions. It is noted that the workspace of a PPM with $\gamma = \alpha_3 = 90$ deg is able to reach the entire pointing workspace instead, which is not shown due to space limit.

B. Velocity analysis

With the velocity equations (45) and (58), the velocities of the five-bar PPM are further simulated. The joint trajectory is specified as $\theta_1 = 3.07 + 0.1\sin(0.04\pi t)$, and $\theta_2 = 2.67 - 0.02t$ in radians, for $t = 0..50$ s, their derivatives giving their velocities.

Using eq. (49), the angular velocity of the mobile platform is readily obtained, as shown in Fig. 7a, while the pointing velocity in terms of changing rates of pointing angles, calculated from eq. (58), is shown in Fig. 7b. Simulation with MSC Adams yielded the same results.

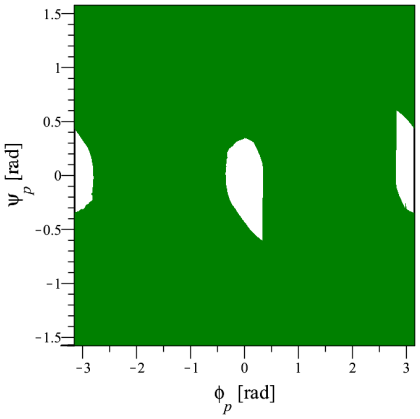

Fig. 6. Pointing workspace of the five-bar PPM, where blank areas are not reachable.

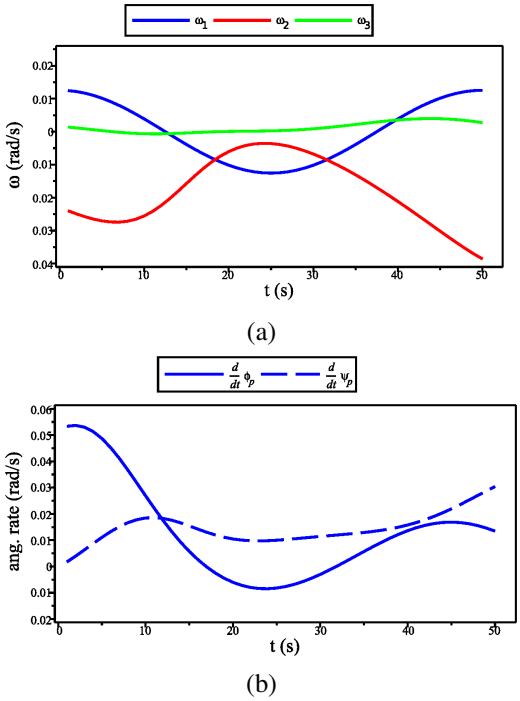

Fig. 7. Velocity analysis of the five-bar PPM, (a) three components of the mobile platform angular velocity, (b) changing rates of pointing angles.

C. 3-RRR PPM

Another example is included for the 3-RRR PPM. The design parameters are given as $(\alpha_1, \alpha_2, \gamma, \beta, \theta_3) = (\pi/4, \pi/2, \pi/4, \pi/3, 7\pi/12)$ rad. Table II lists the complete solutions to forward kinematic analysis for given angles $(\theta_1, \theta_2) = (7\pi/12, \pi/3)$ rad, while Table III provides eight solutions to the inverse problem with $\mathbf{p} = [0.4143, 0.1401, 0.8993]^T$.

D. Performance comparison

The new formulation with the NOF brings computational advantage to the PPM kinematics. To reveal its computational efficiency, tests were conducted for both inverse and forward kinematic problems. In particular, 20 inverse and forward

TABLE II
EIGHT SOLUTIONS OF THE UNIT POINTING VECTOR $\mathbf{p}$

$[-0.8289, -0.4414, -0.3435]$	$[0.4143, 0.1401, 0.8993]$
$[-0.3606, 0.9029, -0.2338]$	$[0.8559, -0.3971, -0.3313]$
$[-0.0200, 0.9624, -0.2710]$	$[0.6967, -0.2490, -0.6727]$
$[-0.7734, -0.6312, 0.05774]$	$[-0.0164, 0.0392, 0.9991]$

TABLE III
EIGHT SETS OF JOINT ANGLES θ_1 AND θ_2 (UNIT: RAD.)

$0.064, 0.602$	$0.064, 2.241$	$2.991, 0.602$	$2.991, 2.241$
$-1.978, -1.740$	$-1.978, 1.046$	$1.832, -1.740$	$1.832, 1.047$

position problems were created separately with data generated randomly within a given workspace. The performance of the NOF formulation is compared with the approach presented in [9] for the five-bar PPM, and with the conventional formulations presented in [21], [22] for the 3-RRR SPM.

As aforementioned, the five-bar PPM admits 2 FK and 4 IK solutions, while the 3-RRR SPM admits 8 solutions for both problems. This means the total numbers of solutions for the four cases are 40, 80, 160, and 160, respectively, upon which the average time for finding single solution is found.

The test results are listed in Table IV. They were obtained with Maple 2019 running on a 64-bit pc with 4-core 1.8Hz CPU. As can be seen in the table, for both the IK and FK problems, the NOF formulation improves significantly computation efficiency. Moreover, the NOF formulation shows superior performance in IK solutions, as it takes less than one tenth of the computation time of other methods. This can be readily explained by the fact that the NOF formulation does not require solving eq. (72) for the orientation of the mobile platform, which reduces the complexity of the system of equations, thus saves computation time.

The new formulation has also advantage to avoid spurious solutions. While the inverse problem of the five-bar PPM admits four solutions, the formulation in [9] can lead to 8 solutions, four of which are spurious as they point to the opposite direction. These spurious solutions are introduced by eq. (72), with which a unit vector of opposite direction to the given one satisfies the equation too. The same problem of spurious solutions exists with the formulation of 3-RRR PPM. In this light, the new formulation is not only efficient, but also robust due to avoiding spurious solutions.

VI. DISCUSSION

While non-orthogonal bases are widely adopted in physics for modeling purpose [19], [23], they are rarely used in robotics. The purpose of this work is to explore the application of non-orthogonal bases as a natural selection of moving frames. As shown in this study, the NOF leads to a small system of constraint equations with minimum variables. The number of variables is equal to two for the five-bar PPM, and three for the 3-RRR PPM. In comparison, the conventional formulations of kinematic constraint equations, as given in Appendix B, have three and five variables, respectively. The NOF formulation hence allows efficient solutions to both forward and inverse kinematic problems, as shown in numerical examples.

TABLE IV
AVERAGE TIME USED FOR FINDING SINGLE SOLUTION

	Five-bar PPM		3-RRR PPM	
	NOF	LCE	NOF	MCCE
IK	0.003 s	0.033 s	0.011 s	0.186 s
FK	0.012 s	0.319 s	0.003 s	0.014 s

LCE: loop-closure equation [9]
MCCE: multi-chain constraint equations [21], [22]

The new formulation is applicable to 2-DOF spherical parallel manipulators with mobile platforms involving rotations in all three axes. Application of such an approach in single DOF mechanisms can be found in [24]. For designs involving rotations in two axes, like the 2-RRR SPM [10] and slider type 2-DOF SPM [11], the rotation matrix requires only two angles of rotation, thus conventional formulations suffice.

In this work, we focus on the new and efficient formulation of kinematic equations. While examples are included to show its advantages in both position and velocity analyses, we do not look into the singularity in this work, as the topic has been intensively studied in literature [25].

VII. CONCLUSIONS

In this work, a new method of alternative rotation representation of moving frames using a non-orthogonal frame (NOF) is proposed. In the work, we introduced the NOF and analyzed its algebraic and geometric properties. Identities for transformation between the NOF and the conventional orthonormal frame were derived. All these theoretical works provide a framework of applying the NOF in the kinematics of PPMs. Examples of the five-bar PPM and 3-RRR PPM demonstrate successfully the application of the NOF formulation.

A major contribution of this work is the NOF formulation for PPMs. With a natural selection of bases, the NOF leads to an elegant formulation of kinematic constraint equations with minimum parameters, which is computational efficient and robust. Moreover, the NOF formulation allows both graphical and analytical workspace analysis to get an overview of the pointing workspace. These advantages of the NOF formulation will be beneficial for PPM design and control.

APPENDIX A
NON-ORTHOGONAL BASIS

Consider a set of n linearly independent vectors $\{\mathbf{e}_k\}$, which are not orthogonal. Any vector $\mathbf{v} \in \mathbb{R}^n$ can be represented uniquely

$$\mathbf{v} = \sum v_k \mathbf{e}_k \tag{64}$$

where v_k are components of $\mathbf{v}$. The components can be calculated by resorting to the reciprocal basis $\{\mathbf{e}^k\}$ of the original basis. The reciprocal basis consists of reciprocal vectors which satisfy

$$\mathbf{e}^i \cdot \mathbf{e}_j = \delta_{ij} \tag{65}$$

where δ_{ij} is the Kronecker delta function. The reciprocal vectors are found as

$$\mathbf{e}^k = (-1)^{k+1} \mathbf{e}_1 \wedge \ldots \wedge \breve{\mathbf{e}}_k \ldots \wedge \mathbf{e}_n / V \tag{66}$$

where the breve indicates that the term $\mathbf{e}_k$ is left out in the wedge product. Moreover, $V = ||\mathbf{e}_1 \wedge \ldots \wedge \mathbf{e}_k \ldots \wedge \mathbf{e}_n||$.

By computing the inner product of $\{\mathbf{e}^k\}$ with the vector $\mathbf{v}$, one gets the components

$$v_k = \mathbf{v} \cdot \mathbf{e}^k \tag{67}$$

In the vector space of $\mathbb{R}^3$, eq. (64) becomes

$$\mathbf{v} = v_1\mathbf{e}_1 + v_2\mathbf{e}_2 + v_3\mathbf{e}_3 \tag{68}$$

with

$$v_i = \mathbf{v} \cdot \mathbf{e}^i; \quad \mathbf{e}^i = \mathbf{e}_j \times \mathbf{e}_k / V \tag{69}$$

where (i, j, k) is a cyclic permutation of $(1, 2, 3)$ and

$$V = ||\mathbf{e}_1 \wedge \mathbf{e}_2 \wedge \mathbf{e}_3|| = \mathbf{e}_1 \cdot (\mathbf{e}_2 \times \mathbf{e}_3) \tag{70}$$

APPENDIX B
CONVENTIONAL FORMULATIONS

A. Five-bar PPMs

This conventional formulation based on loop-closure equation is adopted from [9]. Referring to the PPM of general structure shown in Fig. 2, the loop closure equation is given as

$$(\mathbf{Z}(\theta_1)\mathbf{S}(\alpha_1)\mathbf{Z}(\phi_1)\mathbf{S}(\alpha_3)\mathbf{z}) \cdot (\mathbf{S}(\alpha_0)\mathbf{Z}(\theta_2)\mathbf{S}(\alpha_2)\mathbf{z}) = \cos\alpha_4 \tag{71}$$

where $\mathbf{Z}(\cdot)$ and $\mathbf{S}(\cdot)$ stand for matrices of rotation about z and x axis, respectively. α_0 is the dimension of the curved link B_1B_2. As our interest is the pointing vector, an additional equation is included,

$$\mathbf{p} \times (\mathbf{Q}\mathbf{p}_0) = \mathbf{0} \tag{72}$$

where $\mathbf{p}_0$ is the pointing vector at the reference configuration, $\mathbf{Q}$ is the MP rotation matrix, which can be expressed with Euler angles [9] or as function of θ_1 and ϕ_1 (Fig. 2). Two of the three scalar equations (72) have to be selected for solutions.

In total, we have a system of three scalar equations. In the inverse problem, the unknowns are θ_1 and θ_2, and intermediate variable ϕ_1. In the forward positional problem, unknowns are the unit vector $\mathbf{p}$ and intermediate variable ϕ_1.

B. 3-RRR PPM

Refer to Fig. 4, three constraint equations can be obtained:

$$\mathbf{w}_i \cdot \mathbf{v}_i = \cos\alpha_2, \quad i = 1, 2, 3 \tag{73}$$

Vectors $\mathbf{v}_i$ are expressed through rotation matrix $\mathbf{Q}$ of the mobile platform [3], i.e.

$$\mathbf{v}_i = \mathbf{Q}(\boldsymbol{\phi})\mathbf{v}_{i0} \tag{74}$$

where $\boldsymbol{\phi}$ is the vector of three Euler angles and $\mathbf{v}_{i0}$ the unit vector parallel to the initial position of OA_i.

In addition, eq. (72) is also needed, of which two scalar equations are selected for solutions. In total, a system of five equations is established. They are used to solve inverse problem, with the unknowns of the pointing angles and Euler angles. On the other hand, the forward problem can be solved by the approached reported in [22].

REFERENCES

[1] J. Stuelpnagel. On the parametrization of the three-dimensional rotation group. *SIAM review*, 6(4):422–430, 1964.

[2] J. Angeles and S. Bai. *Kinematics of Mechanical Systems: Fundamentals, Analysis and Synthesis*. Springer, Cham, 2022.

[3] S. Bai, X. Li, and J. Angeles. A review of spherical motion generation using either spherical parallel manipulators or spherical motors. *Mechanism and Machine Theory*, 140:377 – 388, 2019.

[4] C. Chen and D. Jackson. Parameterization and evaluation of robotic orientation workspace: A geometric treatment. *IEEE Transactions on Robotics*, 27(4):656 – 663, 2011.

[5] J. M Hervé. Uncoupled actuation of pan-tilt wrists. *IEEE Transactions on Robotics*, 22(1):56–64, 2006.

[6] W. Li, J. Angeles, and M. Valášek. Contributions to the kinematics of pointing. *Mechanism and Machine Theory*, 108:97–109, 2017.

[7] M. Weck and D. Staimer. Parallel kinematic machine tools – current state and future potentials. *CIRP Annals*, 51(2):671–683, 2002.

[8] T.K. Nagaraja and et al. Design and development of solar panel tracking mechanism. In *Inter. Conf. on Sustainable Engineering and Technology (ICONSET 2018)*, page 020014, 2018.

[9] G. Palmieri, M. Callegari, L. Carbonari, and M.C. Palpacelli. Mechanical design of a mini pointing device for a robotic assembly cell. *Meccanica*, 50(7):1895–1908, 2015.

[10] K. Ueda, H. Yamada, H. Ishida, and S. Hirose. Design of large motion range and heavy duty 2-DOF spherical parallel wrist mechanism. *J. of Robotics and Mechatronics*, 25(2):294–305, 2013.

[11] N. Saiki, K. Tadakuma, and et al. 2-DOF spherical parallel mechanism capable of biaxial swing motion with active arc sliders. *IEEE Robotics and Automation Letters*, 6(3):4680–4687, 2021.

[12] D. Chablat, Michel G, P. Bordure, S. Venkateswaran, and R. Jha. Workspace analysis in the design parameter space of a 2-DOF spherical parallel mechanism for a prescribed workspace: Application to the otologic surgery. *Mechanism and Machine Theory*, 157:104224, 2021.

[13] H. Jeong, S. Baek, W. Kim, and B.-J. Yi. Development of a spherical 2-DOF wrist employing spatial parallelogram structure. In *2020 IEEE/RSJ Int. Conf. on Intelligent Robots and Systems (IROS)*, pages 6434–6439, 2020.

[14] C. M. Gosselin and E. Lavoie. On the kinematic design of spherical three-degree-of-freedom parallel manipulators. *Int. J. of Robotics Research*, 12(4):394–402, 1993.

[15] M. Urizar and M. L. Husty. Assembly mode change of spherical 3-RPR parallel manipulator. *Mechanics Based Design of Structures and Machines*, 40(4):487–505, 2012.

[16] D. Corinaldi, L. Carbonari, and M. Callegari. Optimal motion planning for fast pointing tasks with spherical parallel manipulators. *IEEE Robotics and Automation Letters*, 3(2):735–741, 2018.

[17] X. Li, J. Liu, W. Chen, and S. Bai. Integrated design, modeling and analysis of a novel spherical motion generator driven by electromagnetic principle. *Robotics and Autonomous Systems*, 106:69–81, 2018.

[18] S. Bai. Extended rotation matrix for kinematics of point mechanisms. In O. Altuzarra and A. Kecskemethy, editors, *Advances in Robot Kinematics 2022*, pages 39–46. Springer, Cham, 2022.

[19] C. Doran, S. R. Gullans, A. Lasenby, J. Lasenby, and W. Fitzgerald. *Geometric algebra for physicists*. Cambridge University Press, 2003.

[20] J. Angeles. *Fundamentals of Robotic Mechanical Systems: Theory, Methods, and Algorithms, (Fourth Edition)*. Springer, New York, 2014.

[21] C. M. Gosselin, J. Sefrioui, and M. J. Richard. On the direct kinematics of spherical three-degree-of-freedom parallel manipulators of general architecture. *ASME J. of Mechanical Design*, 116(2):594–598, 1994.

[22] S. Bai, M. R. Hansen, and J. Angeles. A robust forward-displacement analysis of spherical parallel robots. *Mechanism and Machine Theory*, 44(12):2204 – 2216, 2009.

[23] M. G. Genoni and T. Tufarelli. Non-orthogonal bases for quantum metrology. *J. of Physics A: Mathematical and Theoretical*, 52(43):434002, 2019.

[24] S. Bai. Algebraic coupler curve of spherical four-bar linkages and its applications. *Mechanism and Machine Theory*, 158:104218, 2021.

[25] X. Kong. Forward displacement analysis and singularity Analysis of a special 2-DOF 5R spherical parallel manipulator. *Journal of Mechanisms and Robotics*, 3(2), 2011. 024501.